JOURNAL OF PROPULSION AND POWER
Vol. 15, No. 5, September–October 1999

Expansion and Mixing Processes of Underexpanded Supercritical Fuel Jets Injected into Superheated Conditions

Pei-Kuan Wu,* Mehrdad Shahnam,* and Kevin A. Kirkendall†
Taitech, Inc., Dayton, Ohio 45440
Campbell D. Carter‡
Innovative Scientific Solutions, Inc., Dayton, Ohio 45440
and
Abdollah S. Nejad§
U.S. Air Force Research Laboratory, Wright–Patterson Air Force Base, Ohio 45433

The expansion and mixing processes of underexpanded supercritical fuel jets injected into superheated conditions were experimentally studied. Ethylene was used as the fuel, and nitrogen was the ambient gas. The near-field jet plume structure was characterized by the location and size of the Mach disk and the expansion angle. The Mach disk location of the supercritical ethylene jet matches that of an ideal-gas jet. The size of the Mach disk and the expansion angle, however, increase as the injection temperature approaches the critical value. The far-field mixing processes were characterized by measuring fuel mole fraction and temperature distributions using spontaneous Raman scattering. Fuel mole fraction distributions follow a Gaussian function, whereas temperature distributions exhibit a deficit inside the jet plume because of the expansion and acceleration of the fuel jet. As the injection condition approached the critical point, the following observations were made: 1) the ethylene centerline mole fraction increased, 2) the jet width at the stoichiometric level increased, 3) the jet width at half the maximum concentration remained the same, and 4) the temperature deficit became more significant. These results were attributed to the larger injected fuel mass flow and fuel condensation when the jet injection conditions approach the critical point.

Nomenclature

a = distance to jet virtual origin
c = speed of sound
d = injector exit diameter
d_m = diameter of Mach disk
d_{ps} = pseudodiameter
I_s = intensity of scattered signal
k = constant
$\dot{m}$ = fuel mass flow rate
n = number density
P = pressure
R = gas constant
T = temperature
X = fuel mole fraction
x = axial distance from injector exit
x_m = axial distance from injector exit to Mach disk
y = transverse distance from jet centerline
γ = gas specific heat ratio (C_p/C_v)
θ = jet expansion angle at injector exit
μ = fluid viscosity
ρ = fluid density
σ = Raman scattering cross section

Subscripts

CL = jet centerline property
C_2H_4 = property of ethylene
c = property at the critical point
chm = gas property in injection chamber
e = nozzle exit condition
inj = injectant property before reaching nozzle passage
N_2 = property of nitrogen
RAD = radial profile

Introduction

FOR hypersonic flight, e.g., for flight Mach numbers greater than 8, thermal management of the airframe and onboard electronic components is an engineering challenge.[1] Endothermic fuels are currently under evaluation for use as heat absorption media for the airframe and combustor; for these applications, the fuel temperature will be above the critical value before injection. Additionally, the fuel injection pressure will normally be higher than the fuel critical pressure. Thus, the heat management of future aircraft is expected to require fuel injection from supercritical states into superheated environments.[1]

Supercritical fuels are known to exhibit unusual thermophysical and transport properties near their critical point: liquidlike density, zero latent heat, zero surface tension, and high compressibility. These fuels also exhibit large variations in specific heats and speeds of sound, and enhanced values of thermal conductivity, viscosity, and mass diffusivity.[2–4] Previous studies of supercritical fuel injection and atomization processes have been limited in scope and have focused primarily on experiments with injectant temperatures lower than the fuel critical value T_c, into an environment at temperatures higher than T_c.[5–11] These injection processes have been studied in quiescent environments,[5] in supersonic crossflows,[6,7] and in a rocket combustor.[8] Yang et al.,[9] Woodward and Talley,[10] and Mitts et al.[11] investigated liquid droplet combustion and breakup in both subcritical and supercritical environments. These studies all indicate that the injection and mixing processes are not simply fluid dynamics problems; thermodynamic critical anomalies must also be considered.

Received 20 September 1997; revision received 2 November 1998; accepted for publication 2 December 1998.

*Research Scientist, 3675 Harmeling Drive; currently at Kaiser Marquardt, 16555 Saticoy Street, Van Nuys, CA 91406. Member AIAA.
†Research Engineer, 3675 Harmeling Drive.
‡Research Scientist, 2766 Indian Ripple Road. Member AIAA.
§Senior Scientist and Branch Chief; currently at Kaiser Marquardt, 16555 Saticoy Street, Van Nuys, CA 91406.

Wu et al.[12] investigated the injection of ethylene from supercritical into superheated conditions. It was found that the fuel injection follows an isentropic path, and fuel mass flow rates are 20–30% larger than those of ideal-gas jets at the same pressures when the fuel is initially supercritical and near the critical point. In addition, the fuel jet was found to exhibit a long fuel core, starting at the injector exit, which was caused by fuel condensation. The increased mass flow rate and fuel condensation presumably affect the subsequent expansion and mixing processes.

Expansion and mixing characteristics of ideal-gas jets have been studied extensively.[13–17] Crist et al.[14] characterized the near-field jet plume structure with the location and size of the Mach disk. They found that the axial distance to the Mach disk, after normalization by the injector diameter, is proportional to the square root of the ratio of the injection to the ambient pressures. The size of Mach disks of various gases was also measured.[14] Birch et al.[15,16] and Ewan and Moodie[17] studied velocity and concentration decays along the centerlines of underexpanded ideal-gas jets. The decays were correlated, using a pseudodiameter approach, with the pressure ratio and a universal decay constant, as was done for subsonic conditions. Dowling and Dimotakis[18] and Beer and Chigier[19] reviewed the radial mean concentration profiles for subsonic turbulent freejets and found that the concentration distribution follows a Gaussian self-similar solution. Despite these research efforts, however, the structure of an underexpanded jet plume of fuel injected near the critical point has not been investigated.

The objective of this study is thus to characterize the expansion and mixing processes of a supercritical fuel at injection temperatures slightly greater than T_c, with back pressures lower than the critical pressure. Ethylene was used in this study because its critical temperature is near room temperature, and the injection starts from supercritical conditions and is superheated by the end of the process. Measurements were focused on the near-field structure of the expansion plume and far-field characteristics of the mixing process. Test conditions were designed to simulate injection of an endothermic fuel at temperatures between the critical temperature and the point where thermal cracking becomes significant. This paper begins with a description of the experimental methods. Results for the near-field and far-field jet structures are then discussed, treating Mach disk properties, expansion angles, effects of ambient temperature, fuel mole fraction, and temperature distributions. Finally, the differences between the expansion and mixing characteristics of a supercritical fuel and an ideal gas are discussed.

Experimental Methods

Apparatus

The test fluid was injected vertically downward into a large injection chamber filled with an inert gas (nitrogen). Detailed descriptions of the design and operation of the facility have been presented in a previous study.[12] The apparatus consisted of a fuel tank, solenoid valve, fuel temperature control unit, injector, and the injection chamber (Fig. 1). The fuel tank assembly was designed to allow preset initial fuel pressures and temperatures and to provide a steady fuel supply during injection. A solenoid valve with a response time of 150 ms was installed in the fuel delivery line to control the injection duration. Injection times were limited to 5–8 s to minimize fuel consumption and the accumulation of ethylene in the chamber.

The injector passage consisted of a rounded entry and a converging section to ensure that a choke point could occur only at the injector exit. Two injector diameters, 0.5 and 1.0 mm, were tested, and the ratio of passage length to exit diameter was 4 in both cases. The injector design was tested by Wu et al.[12] and has a discharge coefficient of 0.97. The 1.0-mm injector was used for the measurement of the Mach disk structure, whereas the 0.5-mm injector was employed to study 1) the effects of ambient temperature on the near-field expansion process and 2) the far-field mixing characteristics.

Supercritical fuel temperatures were monitored with thermocouples and controlled by flowing ethylene glycol outside the fuel pipe along the fuel delivery line for a distance of over 6 m upstream of the nozzle. Through the use of a heat exchanger, the temperature of the ethylene glycol was maintained at the desired temperature, with an uncertainty of ± 1 K. Tests showed that the final fuel temperature was within 2 K of the coolant temperature; the fuel temperatures reported in this study are therefore the measured coolant temperatures. The fuel static pressure was measured upstream of the nozzle passage with a bridge-type pressure transducer having an uncertainty within ± 7 kPa. The recorded pressure and temperature were then used to quantify the fuel properties before injection.

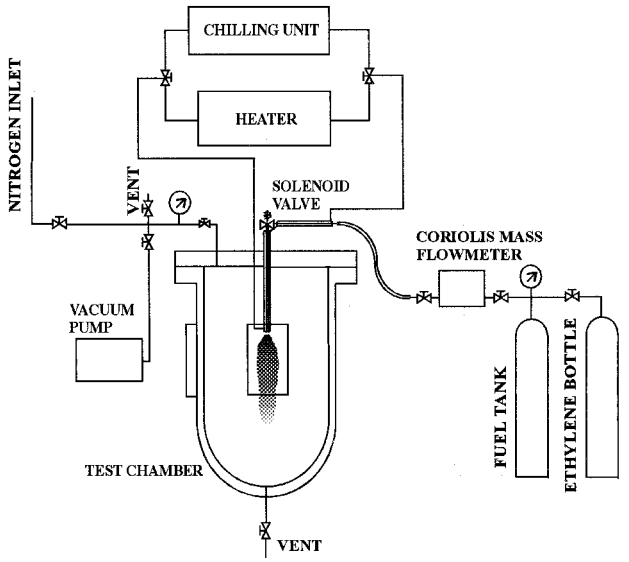

Fig. 1 Sketch of fuel-injection apparatus.

The injection and mixing characteristics of supercritical fuel jets were studied in a large injection chamber. This chamber was designed to simulate temperature and pressure environments encountered in ramjets, scramjets, rockets, and gas turbines, as well as in industrial injector atomization processes. The chamber diameter is 0.42 m and its height is 0.94 m, resulting in an internal volume of 0.12 m^3. Four optical ports are provided for flow diagnostics. The chamber pressure was monitored by a bridge-type pressure transducer, also having an accuracy of ± 7 kPa.

Initially, the chamber was flushed with nitrogen to remove oxygen. The fuel pressure and temperature were set by charging the fuel tank to a specified pressure and adjusting the set temperature of the fuel heat exchanger. Flow was initiated by energizing the solenoid valve; fuel and chamber pressures and temperatures were then recorded by a high-speed data-acquisition board linked to a personal computer. During each run, the rise in chamber pressure was typically less than 34 kPa. After each run, the chamber was vented, flushed, and reset to the desired operating pressure.

To study the effects of ambient temperatures on the near field jet expansion process, electric heaters were used to increase the temperature inside the injection chamber. Four 2.3-kW cartridge heaters were installed inside the chamber to heat the chamber wall temperature to the preset level. Insulation was installed outside the chamber to reduce heat losses. Because of the large thermal mass of the vessel, the fresh nitrogen was readily heated to the preset chamber wall temperature within a short time after it filled the vessel. The gas temperature was thus approximated with a measurement of the chamber temperature T_{chm} and was reasonably constant during the experiment.

Instrumentation

Schlieren Photography

Long-exposure schlieren photographs were taken to resolve shock structures. The schlieren system included a SpeedGraphic camera, loaded with Polaroid type 57 100 × 125 mm black and white film; the shutter speed was $\frac{1}{125}$ s. Two 300-mm-diam parabolic mirrors, with focal lengths of 1220 mm, collimated and focused the light from a mercury lamp. The arrangement provided an image magnification

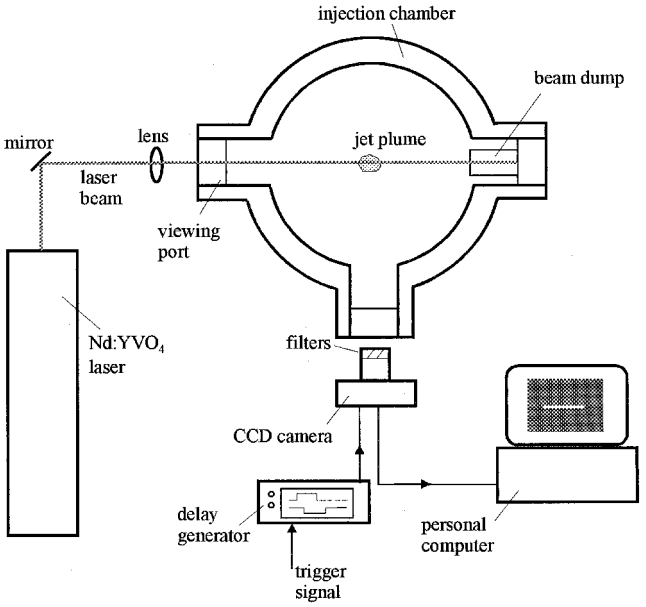

Fig. 2 Sketch of Raman scattering system.

of 4.15 and a 22 × 27 mm field of view (FOV). The location and size of the Mach disk were determined from the photographs by measuring the distance between the center of the Mach disk and the injector orifice and the distance between the two triple points, respectively. The expansion angle was determined as the angle between the jet centerline and the line tangent to the jet boundary passing through the edge of the orifice. Results were obtained by averaging measurements obtained from four photographs for each test condition; measurement uncertainties for the Mach disk size and axial location, and the expansion angle were less than $0.12d$ and 3 deg, respectively. The standard deviation between the four images was less than 4%.

Raman Scattering System

Time-averaged ethylene and nitrogen concentrations along the axis of the laser beam were recorded on an air-cooled, back-illuminated charge-coupled device (CCD), using spontaneous vibrational Raman scattering[20] (see Fig. 2). This CCD camera system, manufactured by PixelVision, Inc., has a high quantum efficiency, ~90% at 600 nm, and low noise, ~11 electrons for a 100-kpixel/s digitization rate; as a consequence, this detector can capture low-level signals such as those from Raman scattering. A continuous wave Nd:YVO_4 laser, the Spectra Physics Millennia, was employed as a light source, and the 3.5-W, 532-nm beam was focused with a 1-m focal length lens into the chamber through a quartz window (Fig. 2). To minimize scattered/reflected light, the second window was replaced by a steel blank incorporating a beam dump. Two optical filter sets were incorporated into the camera system to isolate the Raman signals of ethylene and nitrogen. Each filter set consisted of ~5 mm of colored glass, such as Schott glass OG 570, and an interference filter appropriate for the vibrational Raman shift of the component of interest: 1) for N_2, $\lambda_{center} \cong 610$ vs ~607 nm for the Q-branch band origin; 2) for C_2H_4, $\lambda_{center} \cong 633$ vs 634 nm for the band origin. The purpose of the colored-glass filter was to minimize strong Rayleigh and particle scattering (the Mie scattering signal, e.g., can be many orders of magnitude stronger than the Raman signal). The filter sets, each mounted in a tube having a standard 52-mm external thread, were easily screwed onto the front of the fast Noct Nikkor 58-mm f/1.2 lens, which was used to collect and focus the scattering image onto the CCD array.

The camera was placed just outside the viewing port (see Fig. 2), at a right angle to the laser beam axis. With this setup, the FOV for the 512 × 512 pixel array (24-μm pixels) was ~77 × 77 mm, corresponding to a magnification of ~0.16. Thus, each pixel viewed ~150 μm of physical space. The pixels were binned in the vertical direction (before digitization) because only the variation in concentration along the laser-beam axis was of interest. In all of the measurements, the CCD integrated the Raman scattering signal during a 2-s interval, and the Uniblitz shutter employed by the PixelVision camera was opened following a 1-s delay after initiation of the injection process. The timing of the camera shutter was accurately controlled using a Stanford Research Systems DG535 digital delay generator; a test showed that the accuracy of the shuttering was better than 10 ms. In general, the resulting C_2H_4 Raman scattering signal levels were strong, several thousand counts above the background, and the corresponding photon shot noise for the peak C_2H_4 Raman signals was less than 1%. The camera was carefully focused and squared with respect to the beam axis using scattering from a wire placed in the beam path near the jet centerline. The jet centerline was determined by traversing the laser probe and the camera in concert and finding the maximum C_2H_4 scattering signal. Four images were taken for each test condition, and the average of these images was used to obtain the ethylene and nitrogen number density distributions. The signal variation between images (one standard deviation) was small, corresponding to less than 2 mol/m^3, primarily because of the accumulation of ethylene before (from incomplete purging) and during data collection.

Calibration of Raman Scattering Signals

To determine the number density of both ethylene and nitrogen, it was necessary to establish the relationship between the number density of each gas and the signal recorded by the CCD camera. This calibration was performed by filling the injection chamber with a known concentration of nitrogen and ethylene. Gas number densities were calculated using the ideal-gas state equation based on measured pressures and temperatures. The recorded Raman scattering intensity is plotted in Fig. 3 as a function of the gas number density. The least-squares method was used to determine the proportionality constant and the background level. Correlation coefficients of these tests are both above 99%, and the differences between the fitted and measured background levels are small. Standard errors of estimate of the predictions were found to be 12.6 and 126 counts for nitrogen and ethylene, respectively. The proportionality constants were found to be 470 and 49.6 count/(mol/m^3) for ethylene and nitrogen, respectively. The larger value for ethylene results from the larger Raman scattering cross section ($\sigma_{C_2H_4} = 1.9 \times 10^{-30}$ vs $\sigma_{N_2} = 0.46 \times 10^{-30}$ cm^2/sr at 532 nm),[20] and the fact that the interference filter for ethylene has higher transmission at the Raman scattering wavelength. The linearity of the calibration curve and the close agreement between the measured and fitted background levels validate the present Raman scattering system and indicate that the

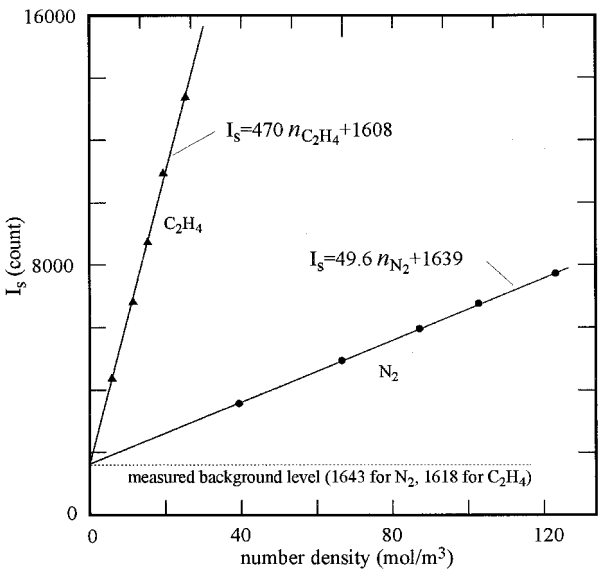

Fig. 3 Calibration of Raman scattering signal vs gas density.

Table 1 Injector exit properties (Refs. 3 and 4) and flow conditions (Ref. 12)[a]

T_{inj}/T_c	P_e/P_{inj}	T_e/T_{inj}	ρ_e, kg/m^3	μ_e, 10^{-7} Pa s	c_e, m/s	γ_e	$(\dot{m}_e)_{meas}$, g/s	R_e, $\times 10^{-6}$
1.04	——	——	——	——	——	——	12.1	——
1.10	0.572	0.878	61.1	113	253	2.17	12.4	1.38
1.14	0.572	0.876	53.2	109	271	1.76	11.6	1.33
1.19	0.572	0.880	47.6	116	287	1.59	10.9	1.18
1.24	0.570	0.884	43.6	119	299	1.50	10.6	1.11
1.27	0.569	0.892	40.5	122	310	1.44	10.4	1.03

[a]Employing 1-mm injector.

filters effectively remove Rayleigh and Mie scattering. The number density of nitrogen and ethylene can thus be determined from the measured signals using these calibrations. The overall uncertainties were calculated using the rss formula, considering the standard deviations of the individual measurements and the calibration uncertainties. The overall uncertainties were 0.16 and 0.44 mol/m^3 for ethylene and nitrogen, respectively.

Test Conditions

The fuel temperature and pressure were set to be slightly above the critical point for studying expansion and mixing characteristics. Ethylene was chosen as a test fuel because its critical temperature is near room temperature, and this reduces the system safety requirements. Nitrogen was used as the ambient gas because it is inert and has properties similar to those of air. Fuel pressures and temperatures are expressed as reduced values, i.e., relative to the critical point values of 5.04 MPa and 282.3 K. The fuel-injection pressure P_{inj} was set between 5.7 and 5.8 MPa, ±1%, yielding reduced pressures from 1.13 to 1.15. Fuel temperatures T_{inj} were varied from 293 to 358 K, resulting in reduced temperatures from 1.04 to 1.27. Chamber pressures P_{chm} were set at 0.14–0.81 MPa. This resulted in jet expansion ratios P_{inj}/P_{chm} of 7.0–56. Chamber temperature T_{chm} was varied from 300 to 447 K, resulting in reduced temperatures from 1.06 to 1.58. Table 1 lists the fluid properties at the injector exit based on the thermophysical properties of Younglove,[4] fluid viscosities from Holland et al.,[3] and the isentropic approximation discussed by Wu et al.[12]

Results and Discussion

Near-Field Mach Disk Structures

Properties of the Mach Disk

Figure 4 shows the near-field expansion of ethylene jets injected into a 0.2-MPa nitrogen environment for injection temperatures of 293, 311, and 354 K, corresponding to reduced temperatures of 1.04, 1.12, and 1.40, respectively. As discussed by Wu et al.,[12] the photograph of the ethylene jet shows a long fuel core caused by fuel condensation, when the injection temperature approaches the critical value. As T_{inj} increases, the fuel condensation is less significant and the Mach disk structure is visible. The bowl shape of the jet plume at the injector exit suggests that a Mach disk exists for the $T_{inj} = 293$ K case, although it is not visible in the photograph. Crist et al.[14] reported that the fuel condensation increases the static pressure inside the jet plume, and a larger Mach disk is thus formed to equalize the pressure field. This fuel condensation core was found to persist for a long distance (about $50d$) before complete evaporation.

The Mach disk locations of the ethylene and nitrogen jets, shown in Fig. 5, are very close, even when the ethylene is injected near the critical point. As P_{inj}/P_{chm} increases, the axial distance from the injector exit to the Mach disk x_m/d increases. This behavior can be predicted by the correlation developed by Crist et al.[14] for an ideal-gas jet injected into an environment of the same gas. This fact suggests that the Mach disk location depends only on the pressure ratio, and is independent of fuel types and fuel condensation. This finding is mentioned by Wu et al.[12] and is quantified in the present study.

Figure 6 shows the diameters of Mach disks d_m/d for the supercritical ethylene and nitrogen jets measured in the present study, along with nitrogen Mach disk diameters from Crist et al.[14] The

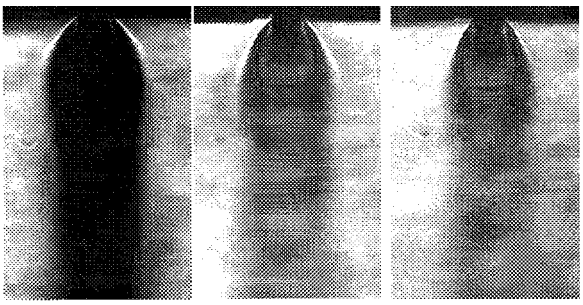

Fig. 4 Effects of injection temperatures on fuel-injection processes.

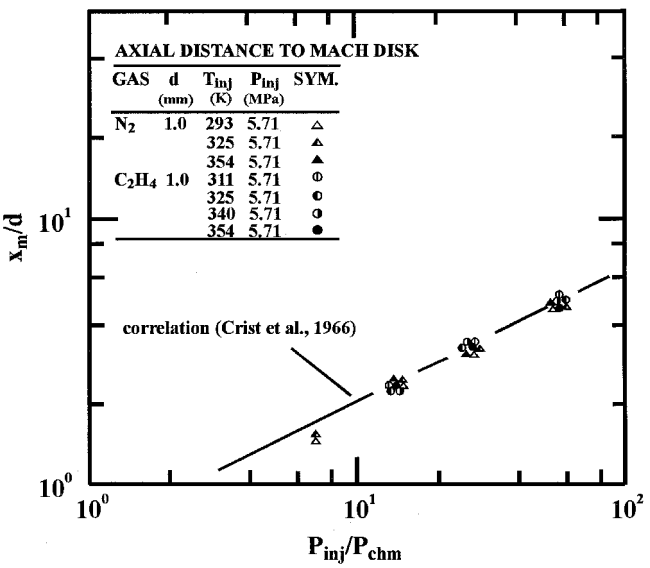

Fig. 5 Locations of Mach disks of ethylene and nitrogen jets.

measurements of Crist et al. agree with the present nitrogen results. These data indicate that d_m/d increases as P_{inj}/P_{chm} increases. Although d_m/d of ethylene jets show the same trend, they are always larger than those of nitrogen jets. For higher injection temperatures ($T_{inj} > 325$ K), d_m/d is fairly constant but 20–30% larger than those of nitrogen jets. Because ethylene takes on the characteristics of an ideal gas when the temperature is much higher than the critical value, the difference in d_m/d was attributed to the difference in ratios of specific heats, γ ($\gamma_{C_2H_4} = 1.22$, and $\gamma_{N_2} = 1.40$).[13,14] For lower injection temperatures ($T_{inj} < 325$ K), however, the d_m/d increases as T_{inj} approaches T_c. At $T_{inj} = 311$ K, d_m is about 10–20% larger than those of ethylene jets at higher T_{inj} and about 40–50% larger than those of nitrogen jets, possibly because of the larger fuel mass and fuel condensation.

The supercritical ethylene jet condenses at $T_{inj} = 293$ K, as shown in Fig. 4, which makes the measurement of Mach disk properties impossible when using the schlieren technique. Therefore, the

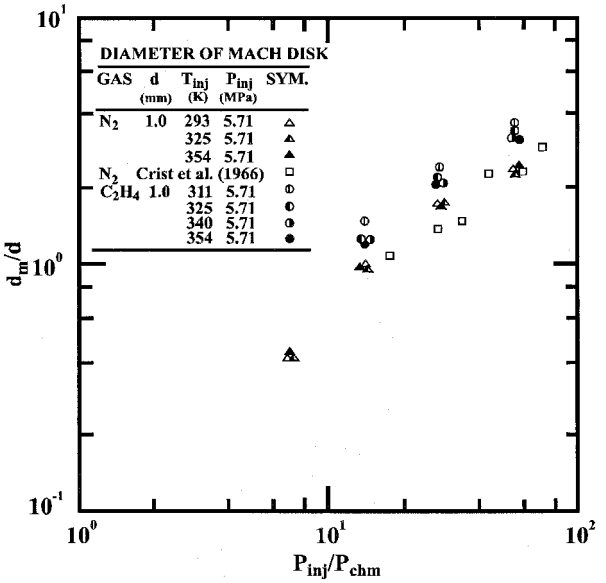

Fig. 6 Diameters of Mach disks of ethylene and nitrogen jets.

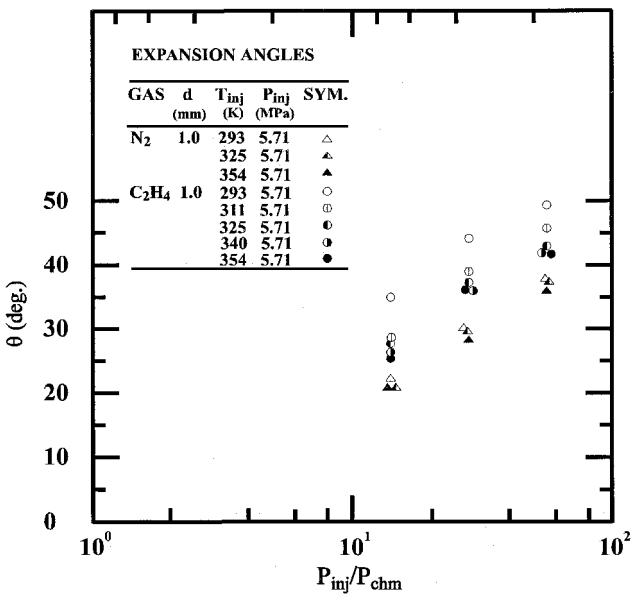

Fig. 7 Expansion angles of ethylene and nitrogen jets.

expansion angle θ is used for comparison. Although the determination of this angle is somewhat subjective, it can provide a good basis for comparison of the degree of expansion for the fuel jets. Figure 7 shows the comparison of expansion angles for nitrogen and ethylene jets. The expansion angle illustrates the same behavior as the Mach disk diameter: the angle increases as $P_{\text{inj}}/P_{\text{chm}}$ increases. For nitrogen jets, θ is insensitive to T_{inj}, even when T_{inj} is varied from 293 to 354 K, perhaps because γ does not change significantly. Ethylene jets always produce a larger θ than nitrogen jets. For higher injection temperatures ($T_{\text{inj}} > 325$ K), the expansion angle is reasonably independent of T_{inj}, as was d_m. For lower injection temperatures ($T_{\text{inj}} < 311$ K), θ increases substantially as T_{inj} decreases, especially when T_{inj} approaches T_c. The expansion angle suggests that d_m at $T_{\text{inj}} = 293$ K will be larger than that at $T_{\text{inj}} = 311$ K.

Effects of Ambient Temperature

Effects of ambient temperature on the near-field Mach disk structure were investigated and are shown in Fig. 8. The injection temperature was kept constant at 293 K, whereas the chamber temperature was varied from 303 to 447 K. These temperatures correspond to T_{inj}/T_c of 1.04 and T_{chm}/T_c from 1.07 to 1.56. For JP-7 fuel

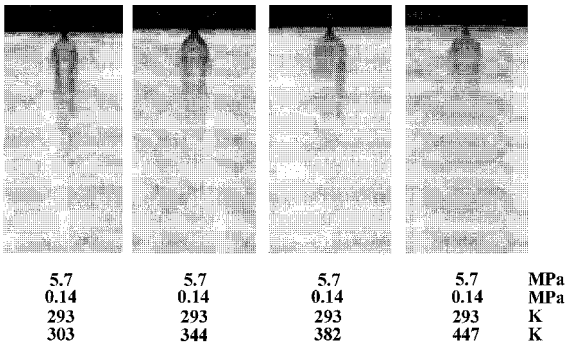

Fig. 8 Effects of ambient temperature on jet plume.

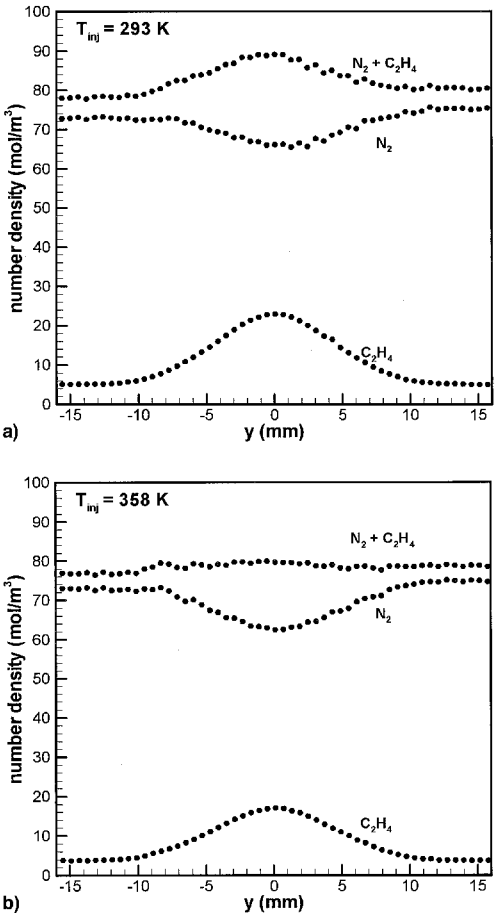

Fig. 9 Measured number density of C_2H_4 and N_2, and the total number density: T_{inj} = a) 293 and b) 358 K.

($T_c = 673$ K),[1] these ranges are equivalent to T_{inj} of 697 K and T_{chm} from 720 to 1050 K, which cover ramjet and scramjet combustor operating conditions.[21] Figure 8 shows that fuel condensation is less significant and the fuel condensation core shortens as the ambient temperature increases. Nevertheless, fuel condensation can still be observed, even at T_{chm} of 447 K, because of the finite heat transfer rate from the ambient gas to the fuel jet plume. It is thus expected that the problem of fuel condensation cannot be neglected, even when the jet is placed in a high-temperature airstream.

Far-Field Mixing Characteristics

The number densities of nitrogen and ethylene, n_{N_2} and $n_{C_2H_4}$, were measured using Raman scattering at $x/d = 112$, $P_{\text{inj}} = 5.8$ MPa, T_{inj} from 293 to 358 K, $P_{\text{chm}} = 0.2$ MPa, and $T_{\text{chm}} = 300$ K. Results for $T_{\text{inj}} = 293$ and 358 K are shown in Figs. 9a and 9b, respectively. The maximum value of ethylene jets is at the jet center and decreases as the radial distance increases. The small amount of

ethylene outside the jet plume resulted from the accumulation of injected ethylene during data acquisition. As expected, n_{N_2} shows a deficit at the jet center because of the presence of the ethylene jet. The sum of n_{N_2} and $n_{C_2H_4}$ yields the total gas number density and exhibits a maximum at the jet centerline at $T_{inj} = 293$ K. Assuming a constant pressure field, this indicates a decrease in the jet center temperature. At $T_{inj} = 358$ K, $n_{C_2H_4}$ is smaller inside the jet plume than the measurements for $T_{inj} = 293$ K. The total gas number density for this case is fairly constant, indicating that the reduction of n_{N_2} at the jet center is compensated for by the presence of $n_{C_2H_4}$. The constant total gas number density is attributed to the higher temperature at the measurement station. The total number density and n_{N_2} show a slight variation across the image domain, possibly because the jet is not perfectly axisymmetric and/or because of laser beam extinction. Note that larger fluctuations in n_{N_2} are a result of the smaller signal-to-noise ratio for nitrogen.

The $n_{C_2H_4}$ and the total number density are used to calculate the fuel mole fraction, which is plotted in Fig. 10 as a function of radial distances for $T_{inj} = 293$, 325, and 358 K. The mole fraction is calculated as

$$X = \frac{n_{C_2H_4} - n_{C_2H_4,b}}{n_{N_2} + n_{C_2H_4}} \tag{1}$$

where $n_{C_2H_4,b}$ is the $n_{C_2H_4}$ accumulated inside the chamber during data collection. The measurement uncertainty of the mole fraction (one standard deviation) was estimated to be 0.004, given the uncertainties in $n_{C_2H_4}$ and n_{N_2}. As shown in Fig. 10, the mole fraction level decreases as T_{inj} increases from 293 to 325 K. As T_{inj} increases from 325 to 358 K, however, the mole fraction distributions do not show significant variations. A stoichiometric mole fraction, 0.065, was also calculated for ethylene in air and is shown in Fig. 10 as the dashed line. A large portion of the jet plume is apparently above the stoichiometric level. The jet width at the stoichiometric level (see Fig. 10) decreases ~7% (14 vs 13 mm) when T_{inj} increases from 293 to 358 K. The larger mole fraction level and jet width for $T_{inj} = 293$ K attributed to the larger fuel mass flow rates, the lower jet temperature and velocity, and the fuel condensation. These distribution curves are smooth and can be fit with a Gaussian function as can a subsonic turbulent freejet.[19]

The temperature distribution of the jet plume was calculated based on the obtained total gas number density and the assumption of a uniform pressure field across the jet plume at the measurement station (Fig. 11). Because the calculated temperature is sensitive to P_{chm}, care was taken to set P_{chm} precisely to a predetermined value. In most instances, P_{chm} was varied within 4 kPa from the predetermined and measured value of 0.2 MPa, to match the calculated temperature outside the jet plume to the measured T_{chm} of about 300 K. The temperature distribution exhibits a deficit within the jet plume because of the expansion process. As T_{inj} increases, the magnitude of the deficit decreases and gradually approaches the ambient temperature (~300 K) at $T_{inj} = 358$ K. The temperature deficit is still

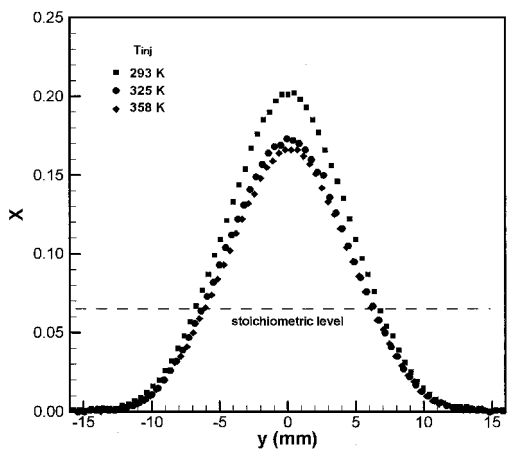

Fig. 10 Mole fractions of ethylene jets at various injection temperatures at $x/d = 112$.

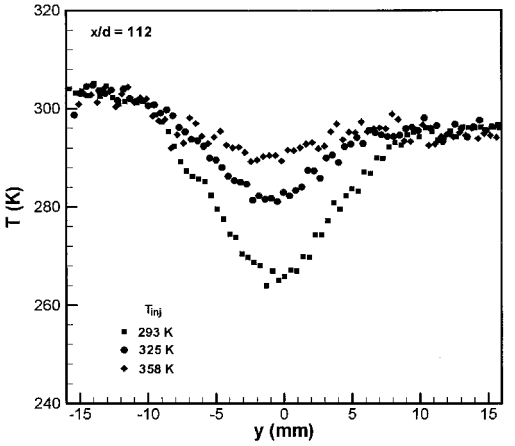

Fig. 11 Temperature distributions of ethylene jets at $T_{inj} = 293$, 325, and 358 K.

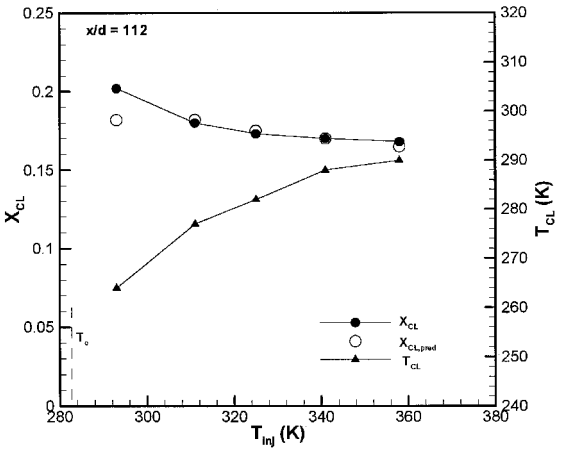

Fig. 12 Variation of the measured and predicted centerline mole fractions and the measured centerline temperatures.

fairly significant at $x/d = 112$ for the $T_{inj} = 293$ K case because of the persistence of near-field expansion and fuel condensation.

The centerline mole fractions and temperatures, X_{CL} and T_{CL}, are shown in Fig. 12 for T_{inj} from 293 to 358 K. X_{CL} decreases and T_{CL} increases as T_{inj} increases from 293 to 325 K; beyond 325 K, the effect of fuel temperature on X_{CL} and T_{CL} is not significant. The thermodynamic critical anomalies and the isentropic injection path approximation[12] suggest that the increase in X_{CL} for $T_{inj} < 325$ K may be attributed to the larger fuel mass flow rates and the smaller speed of sound near the critical point.

Birch et al.[15,16] employed a pseudodiameter approach to predict the centerline mole fraction for underexpanded sonic methane and ethylene jets. The underexpanded fuel jet was treated as a sonic jet injected from a virtual injector. The exit condition at the virtual injector orifice was selected to be ambient pressure and temperature, and the orifice diameter was determined from the conservation of fuel mass. The orifice is termed a pseudodiameter d_{ps}, which replaces d in the decay prediction of a subsonic turbulent jet. This approach was applied with the present results using γ at the injector exit conditions; an X_{CL} value of 0.184 was obtained for all T_{inj} tested. This deficiency was attributed to the fact that the approximation does not consider the thermodynamic critical anomalies. The approach of Birch et al.[15] was then modified using the measured exit conditions, listed in Table 1, to remove the ideal-gas assumption. The resulting correlations for X_{CL} and d_{ps} are

$$X_{CL} = k_{CL}[d_{ps}/(x - a)](\rho_{N_2}/\rho_{C_2H_4})^{\frac{1}{2}} \tag{2}$$

$$d_{ps} = \sqrt{(\rho_e c_e / P_{chm})\sqrt{(RT_{chm}/\gamma)}} \tag{3}$$

Note that the mole fraction is essentially equivalent to the mass fraction for ethylene injection into nitrogen because their molecular weights are virtually identical. The density ratio term in Eq. (2) is unity, and the value of γ in Eq. (3) is equal to 1.22. k_{CL} is the decay constant, which is typically between 4.0 and 5.5 (Ref. 15); 4.2 was used in the present study. As suggested by Birch et al.,[15] the axial distance to the virtual origin a/d was set to be 6.7. The predicted X_{CL} agrees well with the measured values as shown in Fig. 12, except at $T_{inj} = 293$ K. The good agreement indicates that the increase in X_{CL} (except at $T_{inj} = 293$ K) is caused by the increase in fuel mass flow rates because of the rapid increase in fluid density near the critical point.[12] Therefore, the centerline concentration of a supercritical jet injected near the critical point is always higher than that of an ideal-gas jet injected under the same pressures.

At $T_{inj} = 293$ K, the prediction of X_{CL} is about 10% smaller than the measured value. Because the measured mass flow rates (see Table 1) are almost the same for $T_{inj} = 293$ and 311 K, this deficiency is attributed to the presence of fuel condensation at the injector exit. Fuel condensation reduces the jet temperature, and possibly, the velocity. Therefore, the formulations used in the calculation of the speed of sound at the pseudodiameter location and the virtual origin distance to the injector exit may not be valid. Further studies are required to identify the effects of fuel condensation on the jet mixing process and on the centerline concentration decay.

The centerline temperature increases as the injection temperature increases. Because the relative decrease in X_{CL} is at about the same rate as the relative increase in T_{CL} when T_{inj} increases from 325 to 358 K, the increase in T_{CL} is attributed to the mixing process rather than to the increase in T_{inj}. The low T_{CL} measured at T_{inj} of 293 K is related to fuel condensation. If these temperatures scaled with T_c, the present results would correspond to the condition of JP-7 fuel injection at $T_{inj} = 700$ K, $T_{chm} = 713$ K, and $T_{CL} = 626$ K. The low temperatures within the jet plume will increase ignition delay in a combustor and thus affect combustion performance. As the jet stagnation temperature is increased and fuel condensation becomes less significant, T_{CL} gradually approaches the T_{chm} and might be higher than T_{chm} if the stagnation temperature is high enough. Higher ambient temperatures may help to reduce the temperature deficit within a shorter time period, as indicated in Fig. 8. Nevertheless, fuel condensation is still expected to affect the combustion processes because of the finite heat transfer rate from the ambient air to the fuel jet.

The radial ethylene mole fraction profile normalized by the centerline value is plotted in Fig. 13 to check the self-similar characteristics for the cases of $T_{inj} = 293$–358 K. All values collapse onto a single curve and can be modeled well by a Gaussian function. In this study, a least-squares method was applied to find the best fit for $X/X_{CL} > 0.03$. The resulting relation is as follows:

$$\frac{X}{X_{CL}} = \exp\left(-\frac{y^2}{6.34^2}\right) \tag{4}$$

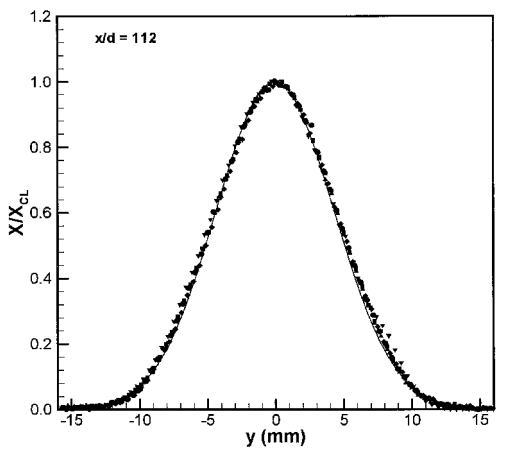

Fig. 13 Measured (symbols) and fitted (solid line) mole fraction distributions of ethylene jets at various injection temperatures.

where the correlation coefficient is 99.5%. The ratio of the predicted to the measured values has a mean of 1.002 with a standard deviation of 0.072. This function demonstrates that the full width at half the maximum concentration of these normalized mole fractions is 10.5 mm. Equation (2) can be written in a self-similar form as

$$X/X_{CL} = \exp\left\{-k_{RAD}[y/(x-a)]^2\right\} \tag{5}$$

where x is 55.9 mm in the present case, and k_{RAD} is a radial spread constant. Beer and Chigier[19] suggested $k_{RAD} = 54$–57 for subsonic turbulent freejets, and the agreement with the profile of Dowling and Dimotakis[18] is reasonable for y/x less than 0.15. In the present study, k_{RAD} was found to be 69. The larger constant indicates that the radial concentration profile is narrower after normalization for an underexpanded jet than for a subsonic turbulent freejet, presumably because of the expansion process.

The mole fraction profile of ethylene jets shows a larger centerline fuel mole fraction, a greater jet width, and a lower centerline temperature at the same axial location when the injection temperature approaches the critical value. These phenomena are related to thermodynamic critical anomalies and fuel condensation. Care, however, has to be taken when applying the mixing efficiency criteria developed from the results of noncondensing ideal-gas jets to supercritical fuel jets.[22] According to these criteria, a larger centerline concentration indicates less mixing, whereas a larger jet plume area implies better efficiency. These criteria apparently should be modified for fuel jets at conditions where thermodynamic critical anomalies or fuel condensation are significant. The effects of these phenomena on the combustion process should also be addressed in future studies.

Summary and Conclusions

Expansion and mixing processes of fuel jets injected from supercritical to superheated conditions were studied. The location and size of the Mach disk, expansion angle, fuel mole fraction, and temperature distributions were characterized using schlieren photography and spontaneous Raman scattering. The major conclusions are as follows:

1) Near the nozzle exit, supercritical ethylene jets exhibited an opaque region at low T_{inj}, which persisted for a distance of about 50 injector diameters. This opaque region, which is caused by fuel condensation, disappears as the injection temperature increases. Nevertheless, the fuel jet still undergoes the expansion process and exhibits a bowl-shaped jet boundary at the injector exit.

2) The Mach disk location of a supercritical ethylene jet agreed with that of an ideal-gas jet. The size of the Mach disk and the expansion angle, however, increased as the injection temperature approached the critical value, possibly because of the larger injected fuel mass and condensation.

3) A higher ambient temperature reduced the length of the fuel condensation core, although fuel condensation was still observed even at high ambient temperatures. This is attributed to the finite heat transfer rate from the ambient gas to the jet plume.

4) The mole fraction distribution of ethylene, determined from Raman scattering, has a maximum value at the jet center and can be modeled by a Gaussian function, in spite of the near-field fuel condensation and thermodynamic critical anomalies. The spread of the jet plume after normalization by the centerline value, however, is smaller than that of a subsonic turbulent freejet.

5) The centerline concentration can be predicted using a pseudodiameter approach when the critical point properties and an isentropic injection path are applied. The prediction indicates that the centerline concentration of a supercritical jet injected near the critical point is higher than that of an ideal-gas jet injected at the same pressure. This phenomenon is caused by the larger injected mass flow rate because of the rapid increase in fuel density near the critical point. The prediction, however, underestimates the centerline value for cases in which fuel condensation is significant.

6) The temperature distribution exhibited a modest deficit in the jet plume because of the expansion process. The deficit became

significant, however, when the injection temperature approached the critical value, because of the fuel condensation.

Acknowledgments

This work was supported by and performed at the U.S. Air Force Research Laboratory, Wright–Patterson Air Force Base, Ohio under Air Force Contracts F33615-96-C-2614 and F33615-97-C-2702. The authors would like to thank M. R. Gruber, J. M. Donbar, and R. P. Fuller for helpful discussion; and the assistance of A. E. S. Creese for editorial comments concerning the paper is appreciated.

References

[1]Edwards, T., "USAF Supercritical Hydrocarbon Fuels Interests," AIAA Paper 93-0807, Jan. 1993.

[2]Nieto de Castro, C. A., "Thermal Conductivity and Thermal Diffusivity in Supercritical Fluids," *Supercritical Fluid Technology: Reviews in Modern Theory and Applications*, edited by T. J. Bruno and J. F. Ely, CRC Press, Boca Raton, FL, 1991, Chap. 9.

[3]Holland, P. M., Eaton, B. E., and Hanley, H. J. M., "A Correlation of the Viscosity and Thermal Conductivity Data of Gaseous and Liquid Ethylene," *Journal of Physical and Chemical Reference Data*, Vol. 12, No. 4, 1983, pp. 917–932.

[4]Younglove, B. A., "Thermophysical Properties of Fluids: I. Argon, Ethylene, Parahydrogen, Nitrogen, Nitrogen Trifluoride, and Oxygen," *Journal of Physical and Chemical Reference Data*, Vol. 11, Suppl. 1, 1982, pp. 58–96.

[5]Chen, L. D., "Heat Transfer, Fouling, and Combustion of Supercritical Fuels," Univ. of Iowa, F49620-92-J-0462, Iowa City, IA, 1994, pp. 6–25.

[6]Hermanson, T. C., Papas, P., and Kay, I. W., "Structure and Penetration of a Transverse Fluid Jet Injected at Supercritical Pressure into Supersonic Flow," AIAA Paper 92-3652, July 1992.

[7]Hendricks, R. C., Boldman, H. E., Neumann, H. E., and Vlcek, B. L., "Quantitative Investigation of Fluid Injection into a Supersonic Flow Field," *Advances in Cryogenic Engineering*, Vol. 35, edited by R. W. Fast, Plenum, New York, 1990, pp. 469–476.

[8]Mayer, W., and Tamura, H., "Propellant Injection in a Liquid Oxygen/Gaseous Hydrogen Rocket Engine," *Journal of Propulsion and Power*, Vol. 12, No. 6, 1996, pp. 1137–1147.

[9]Yang, V., Hsiao, G. C., Shuen, J.-S., and Hsieh, K.-C., "Droplet Behavior at Supercritical Conditions," *Recent Advances in Spray Combustion: Spray Atomization and Drop Burning Phenomena*, Vol. 171, edited by K. K. Kuo, Progress in Astronautics and Aeronautics, AIAA, Reston, VA, 1996, pp. 413–437.

[10]Woodward, R. D., and Talley, D. G., "Raman Imaging of Transcritical Cryogenic Propellants," AIAA Paper 96-0468, Jan. 1996.

[11]Mitts, C., Talley, D. G., and Poulikakos, D., "A Fundamental Study of Supercritical Droplet Deformation and Breakup Through a Miscible Fluid Analog," AIAA Paper 96-2858, July 1996.

[12]Wu, P.-K., Chen, T. H., Nejad, A. S., and Carter, C. D., "Injection of Supercritical Ethylene in Nitrogen," *Journal of Propulsion and Power*, Vol. 12, No. 4, 1996, pp. 770–777.

[13]Adamson, T. C., and Nicholls, J. A., "On the Structure of Jets from Highly Underexpanded Nozzles into Still Air," *Journal of Aerospace Sciences*, Vol. 26, No. 1, 1959, pp. 16–24.

[14]Crist, S., Sherman, P. M., and Glass, D. R., "Study of the Highly Underexpanded Sonic Jet," *AIAA Journal*, Vol. 4, No. 1, 1966, pp. 68–71.

[15]Birch, A. D., Brown, D. R., Dodson, M. G., and Swaffield, F., "The Structure and Concentration Decay of High Pressure Jets of Nature Gas," *Combustion Science and Technology*, Vol. 36, Nos. 5, 6, 1984, pp. 249–261.

[16]Birch, A. D., Hughes, D. J., and Swaffield, F., "Velocity Decay of High Pressure Jets," *Combustion Science and Technology*, Vol. 52, No. 1–3, 1987, pp. 161–171.

[17]Ewan, B. C. R., and Moodie, K., "Structure and Velocity Measurements in Underexpanded Jets," *Combustion Science and Technology*, Vol. 45, Nos. 5, 6, 1986, pp. 275–288.

[18]Dowling, D. R., and Dimotakis, P. E., "Similarity of the Concentration Field of Gas-Phase Turbulent Jets," *Journal of Fluid Mechanics*, Vol. 218, Sept. 1990, pp. 109–141.

[19]Beer, J. M., and Chigier, N. A., *Combustion Aerodynamics*, Krieger, Malabar, FL, 1983, pp. 10–12.

[20]Eckbreth, A. C., *Laser Diagnostics for Combustion Temperature and Species*, Abacus Press, Cambridge, MA, 1988, pp. 162–219.

[21]Tishkoff, J. M., Drummond, J. P., Edwards, T., and Nejad, A. S., "Future Direction of Supersonic Combustion Research: Air Force/NASA Workshop on Supersonic Combustion," AIAA Paper 97-1017, Jan. 1997.

[22]Fuller, R. P., Wu, P.-K., Nejad, A. S., and Schetz, J. A., "Comparison of Physical and Aerodynamic Ramps as Fuel Injectors in Supersonic Flow," *Journal of Propulsion and Power*, Vol. 14, No. 2, 1998, pp. 135–145.